Li *et al. Plant Methods* (2025) 21:73
https://doi.org/10.1186/s13007-025-01398-1

Plant Methods

RESEARCH Open Access

Unified estimation of rice canopy leaf area index over multiple periods based on UAV multispectral imagery and deep learning

Haixia Li[1], Qian Li[2], Chunlai Yu[1] and Shanjun Luo[2,3*]

Abstract

Background Rice is one of the major food crops in the world, and the monitoring of its growth condition is of great significance for guaranteeing food security and promoting sustainable agricultural development. Leaf area index (LAI) is a key indicator for assessing the growth condition and yield potential of rice, and the traditional methods for obtaining LAI have problems such as low efficiency and large error. With the development of remote sensing technology, unmanned aerial multispectral remote sensing combined with deep learning technology provides a new way for efficient and accurate estimation of LAI in rice.

Results In this study, a multispectral camera mounted on a UAV was utilized to acquire rice canopy image data, and rice LAI was uniformly estimated over multiple periods by the multilayer perceptron (MLP) and convolutional neural network (CNN) models in deep learning. The results showed that the CNN model based on five-band reflectance images (490, 550, 670, 720, and 850 nm) as input after feature screening exhibited high estimation accuracy at different growth stages. Compared with the traditional MLP model with multiple vegetation indices as inputs, the CNN model could better process the original multispectral image data, effectively avoiding the problem of vegetation index saturation, and improving the accuracies by 4.89, 5.76, 10.96, 1.84 and 6.01% in the rice tillering, jointing, booting, and heading periods, respectively, and the overall accuracy was improved by 6.01%. Moreover, the model accuracies (MLP and CNN) before and after variable screening showed noticeable changes. Conducting variable screening contributed to a substantial improvement in the accuracy of rice LAI estimation.

Conclusions UAV multispectral remote sensing combined with CNN technology provides an efficient and accurate method for the unified multi-period estimation of rice LAI. Moreover, the generalization ability and adaptability of the model were further improved by rational variable screening and data enhancement techniques. This study can provide a technical support for precision agriculture and a more accurate solution for rice growth monitoring. More feature extraction and variable screening methods can be further explored in future studies by optimizing the model structure to improve the accuracy and stability of the model.

Keywords Leaf area index, Precision agriculture, Drones, Multispectral imagery, Rice

*Correspondence:
Shanjun Luo
luoshanjun@hnas.ac.cn
[1]Huanghe University of Science and Technology, Zhengzhou 450006, China
[2]Aerospace Information Research Institute, Henan Academy of Sciences, Zhengzhou 450046, China
[3]School of Remote Sensing and Information Engineering, Wuhan University, Wuhan 430079, China

Background

Rice, as the main source of food for more than half of the world's population, is not only a key crop for sustaining human survival and development but also an important component of the agricultural economy [1]. Rice growth monitoring is a key link in ensuring food security and promoting sustainable agricultural development [2]. By dynamically grasping the growth status of rice, it can guide field management, improve yields, and reduce the impact of human activities on the environment [3]. Furthermore, monitoring rice growth can reveal the response of rice to climate change, promote the development of adapted varieties and cultivation techniques, and ensure stable yields and farmer returns [4]. The leaf area index (LAI) reflects the crop canopy's ability to intercept light energy, which directly affects the photosynthetic efficiency and dry matter accumulation of the crop, thus determining the final crop yield [5]. Rice LAI is a key indicator for assessing crop growth and yield potential, and is useful for guiding scientific water and fertilizer management, pest and disease control, and other field management measures [6].

Traditional techniques for obtaining rice LAI mainly include direct measurement and leaf area meter methods. The direct measurement method involves measuring the length and width of leaves and then multiplying them to obtain leaf area [7]. The results obtained by this method are subject to large errors and are usually not representative of the distribution of LAI within a region. The leaf area meter method involves separating stems and leaves indoors by selecting a certain number of plants at each stage. The leaf area of each leaf is then measured by instrument scanning. Finally, the LAI is calculated from the cumulative leaf area and planting density [8]. Although these methods can directly determine the LAI of crops in a small area, they are damaging to plants and time-consuming [9]. With the development of remote sensing technology, the method of non-contact measurement for LAI estimation has gradually become a hot spot for research and application. In recent years, with the development of sensor technology, remote sensing images acquired based on unmanned aerial vehicles (UAVs) have higher spatial and temporal resolution compared with satellite remote sensing images [10]. Compared with RGB and hyperspectral sensors, UAV multispectral cameras can be used to acquire multi-band (from visible to near-infrared) remote sensing data with high spatial resolution (centimeter level) and can achieve a balance between cost and availability [11]. These advantages enable it to show great potential for applications in agriculture, forestry, ecology, environment, and other fields [12].

Canopy spectra are closely related to rice growth because rice canopy reflectance carries valuable information about the interaction of the canopy with solar radiation [13]. In the visible range, rice strongly absorbs sunlight and exhibits low reflectance due to the presence of pigments (chlorophyll, carotenoids and anthocyanins, etc.). In the near-infrared (NIR) range, canopy reflectance exhibits relatively high values due to the influence of thick plant tissues and canopy structure [14]. Optical vegetation indices based on combinations of reflectance in different bands are widely used for LAI extraction in the field and regions [15]. Empirical models based on vegetation indices are difficult to apply in practice mainly for two reasons. First, in the early stage of rice growth, the influence of water and soil background makes the obtained crop canopy information inaccurate. Since the rice LAI is small in the seedling period, the proportion of the bare background of the field canopy is large. At this time, the leaves mainly show lateral growth, while the soil and rice have different spectral characteristics, and the direct use of canopy spectra for LAI estimation is bound to have a large error [16]. Second, the canopy leaves gradually increased in the middle and late stages of rice growth, mainly showing vertical growth. The saturation of the vegetation index makes the canopy LAI estimation accuracy limited and it is difficult to detect changes in LAI. In addition to the vegetation index, information such as height [17], texture [18], and temperature [19] proved to be good auxiliary effects in the extraction of crop growth parameters. On the one hand, the extraction of this information inevitably increases the complexity and cost of the UAV. On the other hand, most studies have fused different types of variables using multiple regression, machine learning, or deep learning. This fusion is mechanistically difficult to explain and the models are less generalizable across time.

Crop LAI estimation is one of the hot spots in agricultural quantitative remote sensing research. Currently, there are mainly physical modeling and empirical modeling methods to obtain LAI by remote sensing. The core of physical model inversion method is the radiative transfer model (RTM).The most representative model of RTM is the PROSAIL model [20]. For example, when the Look up table (LUT) method was used for LAI inversion, it was found to be more accurate than the iterative optimization technique and neural network method [21]. In rice LAI estimation, higher accuracy was achieved when combining PROSAIL and Bayesian network models [22]. However, disease inversion is an important obstacle in RTM-based estimation of vegetation growth parameters. Furthermore, although the physical mechanism of the RTM method is clear and the model is robust, it requires numerous parameters and the process is complicated, which is not convenient for practical application.

In recent years, deep learning technology has reconstructed the three core task frameworks of remote

sensing image analysis - pixel-level segmentation, region-level classification and regression modeling. Its core advantage lies in breaking through the dependence of traditional methods on artificial feature engineering through an end-to-end feature learning mechanism, and realizing autonomous resolution of complex feature patterns and multi-scale spatial associations. For remote sensing image data, convolutional neural networks (CNNs) are often used to accomplish the classification task for multispectral and hyperspectral images [23–25].The application of CNNs avoids the feature loss caused by manual extraction, and provides an alternative method to automatically learn rich features from large raw image datasets. For example, AI-based deep learning has been proposed for updating and digitizing cadastral maps, achieving a notable intersection over union score of 92% [26]. For textual data, deep neural networks based on multilayer perceptrons are extracted widely used for data fusion. For example, multimodal remote sensing features were fused by DNN model to accurately predict soybean yield [19]. Moreover, the fusion of LSTM models enhances the capture of time series data [27]. However, most of the CNN models in the above studies were based on lower spatial resolution dominated satellite remote sensing images as the data base. MLP-based data, on the other hand, focuses on textual data. Deep learning-based automatic feature extraction and regression modeling of UAV high-resolution image data have yet to be studied in depth.

Given the above advantages of deep learning (extraction of deep features) and the shortcomings of the traditional vegetation index method (saturation in the middle and late stages), the present study proposes to use a deep learning method to extract the subtle change features in the original remote sensing reflectance images with a view to improving the accuracy of rice LAI estimation over multiple periods. The extracted vegetation indices (textual information) and reflectance imagery (image information) were used as the data base to fully explore the role of different information in estimating rice LAI. Based on the existing commonly used MLP and CNN, only the UAV multispectral image information was utilized in this study to explore the construction of a multi-period adaptive estimation model for rice LAI based on deep learning. The main objectives are (1) to construct a rice LAI estimation model for different periods by fusing different vegetation indices using MLP; (2) to mine spectral reflectance image information using CNN to construct a unified estimation model for rice LAI in multiple periods; (3) to compare the effects of different input variables on the accuracy of MLP and CNN models; and (4) to compare the accuracy of estimating rice LAI with traditional machine learning models.

Methods

Experimental arrangements

This study included two controlled nitrogen fertilizer experiments located in Hubei and Hainan Provinces. Experiment 1 (Fig. 1(b)) was conducted in 2022 and was divided into three equal-sized and identical-shaped plots (each plot was about 135 m^2 in size). Each plot was further divided into nine plots, with each plot having an area of about 15 m^2. Three representative hybrid rice varieties, i.e., Luoyou 9348, Fengshioyou 4, and Changshioyou

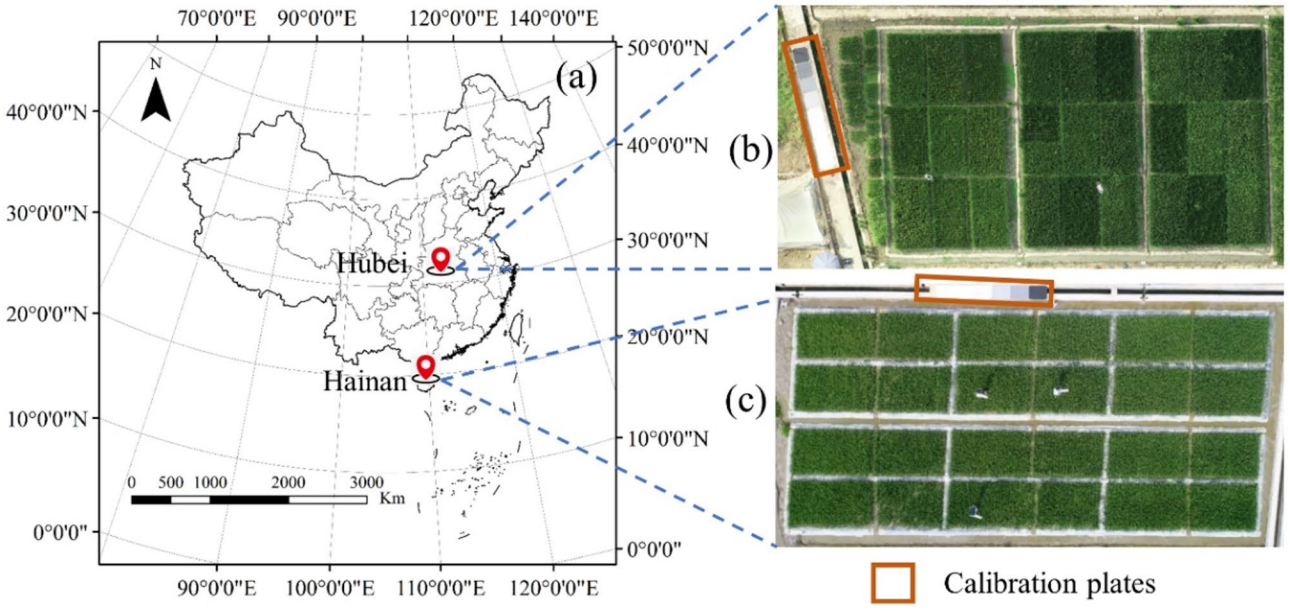

Fig. 1 Experimental area and plots layout: (**a**) experimental location; (**b**) the controlled trial in 2022; and (**c**) the controlled trial in 2018

582, were planted in these plots, and each variety was replicated three times. Three nitrogen fertilizer levels (36, 144, and 288 kg/ha) were set in this experiment, and the same level of nitrogen was applied to each plot. Experiment 2 (Fig. 1(c)) was performed in 2018 and contained a total of 24 plots (the area of each plot was kept the same as in Experiment 1). Four nitrogen gradients (0, 120, 180, and 240 kg/ha) were set up in this experiment, and two different rice varieties, Luoyou 9348 and Fengtiyou No. 4, were planted in three replications. In the two N gradient experiments, white plastic films were placed between the plots at different nitrogen application levels to isolate the water and fertilizer. The field management of the experimental area was handled by specialized personnel, and the yield was not affected by factors such as insect pests and weeds. The control variable in this experiment was the nitrogen application level, and the other field management in each plot was consistent with each other except for the different amounts of nitrogen fertilizer.

Acquisition and processing of UAV multispectral images

The UAV remote sensing data for this study were acquired by a UAV-mounted MCA multispectral camera (Tetracam, Inc., Chatsworth, CA, USA), and the UAV system used for remote sensing image acquisition is shown in Fig. 2. The MCA camera consists of 12 individual lenses with a wavelength range of 490–950 nm, which covers the widely used visible to near-infrared bands that are widely used in precision agriculture. The UAV mission was selected under clear, cloudless, and windless conditions. Multispectral image processing includes three parts: geometric processing, radiometric processing, and spectral information extraction. The geometric processing includes vignetting correction, band alignment, and aberration correction, which was accomplished in the dedicated processing software PixelWrech 2 (Tetracam, Inc., Chatsworth, CA, USA). Radiometric calibration is an important factor in determining the accuracy of spectra and their derivatives (e.g., VI) [28, 29]. Eight calibration plates with known reflectance (reflectance of 3, 6, 12, 24, 36, 48, 56, and 80%, respectively) and the piecewise empirical line (PEL) method

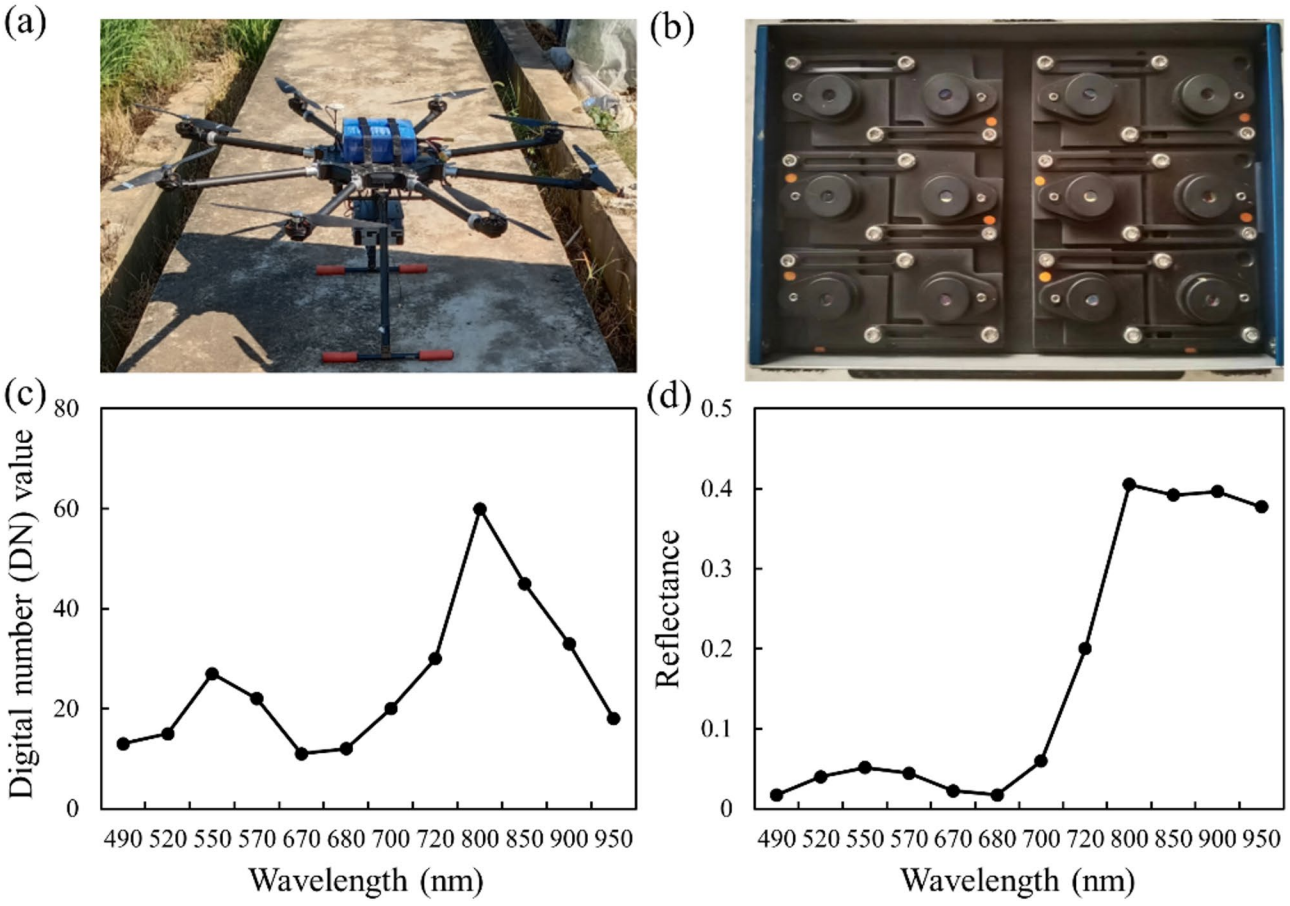

Fig. 2 Unmanned aerial systems and multispectral image processing: (**a**) unmanned aerial systems; (**b**) MCA-12 multispectral camera; (**c**) DN values of canopy images before radiometric calibration at the TS; (**c**) canopy reflectance after radiometric calibration at the TS

were used to perform radiometric calibration to obtain high-precision canopy spectra [30]. The changes in the canopy spectral curves of rice before and after calibration at the TS are shown in Fig. 2 (c-d). It can be seen that the spectral curves of the rice canopy before radiometric calibration were generally different from the typical spectral curves of vegetation, especially in the near-infrared band. The spectral profile after radiometric calibration, on the other hand, conforms to the spectral profile of normal vegetation. Canopy reflectance at the rice plot level was obtained from the UAV images by defining a rectangular region of interest (ROI). The time of UAV data acquisition included rice tillering, jointing, booting, and heading stages. The UAV data acquisition time was between 10:00 and 14:00. UAV flight altitude was set to 60 m in the 2022 experiment and 50 m in the 2018 experiment. The date of UAV data acquisition was aligned with subsequent LAI measurements.

LAI measurements

LAI measurements can be divided into non-destructive and destructive measurements. Non-destructive measurements are generally performed using the LAI2200C canopy analyzer (LI-COR, Lincoln, Nebraska, USA) or the SUNSCAN canopy analysis system (Delta Inc., UK). However, this method requires certain light conditions and is generally only suitable for LAI measurements of sparsely growing plants. In the case of rice, the continuous growth of leaves inside the canopy even after canopy closure and the emergence of spikes after heading can result in low LAI values from non-destructive measurement methods. The destructive method of measuring LAI was used with LI3100C (LI-COR, Lincoln, NE, USA). Before measurements, rice plants were randomly sampled in three holes in each plot in the field, and the green leaves were cut off one by one when they returned indoors. At the late stage of rice growth, the yellow leaves will be removed, and then all the leaves will be scanned one by one to obtain the leaf area of rice per hole, which will then be converted with the rice planting density to finally obtain the LAI of each plot [22]. This destructive measurement method is a cumbersome process, but it can obtain a more accurate LAI value, so this method was used in this study for the measurement of rice LAI in different periods. LAI measurements covered a total of four stages of rice growth (tillering stage (TS), jointing stage (JS), booting stage (BS), and heading stage (HS)). In the 2022 experiment, LAI measurements were taken on July 2, July 11, July 22, and August 15, in that order. In the 2018 experiment, LAI measurements were taken on February 12, February 20, March 11, and April 1, in that order. All LAI measurements were taken between 8:30 – 9:30 AM and 4:00–5:00 PM.

Table 1 Vegetation indices for rice LAI Estimation

Name	calculation	Reference
Difference vegetation index (DVI)	R_{850nm}-R_{670nm}	[31]
Ratio vegetation index (RVI)	R_{850nm} / R_{670nm}	[32]
Normalized difference vegetation index (NDVI)	(R_{850nm}-R_{670nm})/ (R_{850nm} + R_{670nm})	[33]
Normalized difference red-edge vegetation index (NDRE)	(R_{850nm}-R_{720nm})/ (R_{850nm} + R_{720nm})	[34]
Visible atmospherically resistant index (VARI)	(R_{550nm}-R_{670nm})/ (R_{550nm} + R_{670nm})	[35]
Two-band enhanced vegetation index (EVI2)	2.5*(R_{850nm}-R_{670nm})/ (R_{850nm} + 2.4*R_{670nm} + 1)	[36]
Wide dynamic range vegetation index (WDRVI)	(0.2*R_{850nm}-R_{670nm})/ (0.2*R_{850nm} + R_{670nm})	[37]

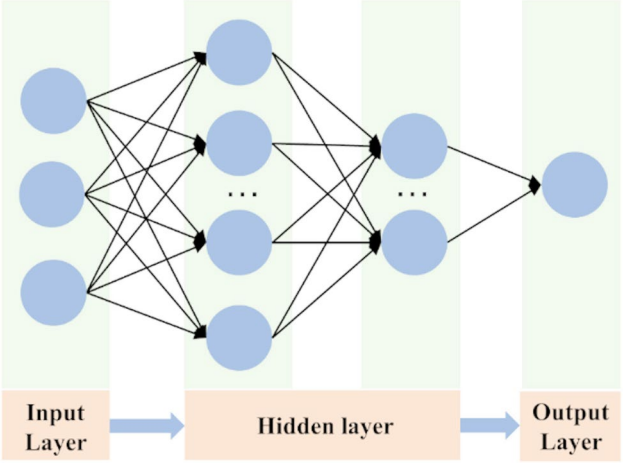

Fig. 3 Architecture of the multilayer perceptron network

Calculation of vegetation indices

Vegetation indices based on spectral reflectance calculations (in two or more bands) have been shown by many scholars to be effective in monitoring vegetation growth due to their ability to enhance vegetation characteristics. In this study, twelve vegetation indices with good performance in existing related studies were selected for the estimation of rice LAI. The calculation of vegetation indices is shown in Table 1.

Deep learning and model evaluation

The MLP network model is a global approximation of a nonlinear mapping, and each of its internal parameters has an equal status on the output of the network, which is commonly used for data estimation and mining in agriculture [38]. Based on the relationship of the data samples in this study, an MLP model consisting of an input layer, two hidden layers, and an output layer was proposed, with the structure shown in Fig. 3. The rectified linear unit (ReLU) was utilized as the activation function, and the network model was trained using the Adam optimizer with a maximum training periods of 200.

In this study, a CNN model was developed to extract deep features from multispectral images, and the rice LAI was estimated based on these features. Due to the small size of the original input image in the sampling area, to minimize the loss of image information, the feature extraction and dimensionality reduction of the image data were performed only by the convolutional layer without pooling layers and up- and down-sampling operations. Finally, the LAI was estimated by the fully connected layer. The model took the canopy spectral reflectance image as input, and the base structure of the network was the Conv block, which consisted of the Conv2d layer, the BN (BatchNorm2d) layer, and the ReLU activation layer. During the network design process, a convolution kernel of small size was used as much as possible to enhance the extraction of local detailed features of the image, and the model convolution process is shown in Fig. 4. In order to obtain the optimal model and to ensure that the model loss value dropped to a low level and converged, the mean square error was used as the loss function, ReLU as the activation function, the maximum training period was 1000, the number of batches was 3, and the initial learning rate was 0.3. The learning rate during the training process was calculated using a step-updating strategy, and the calculation formula for the learning rate in each generation is shown in Eq. (1).

$$L_i = \beta L_{i-1} \tag{1}$$

where L_i is the learning rate of generation i, L_{i-1} is the learning rate of generation i-1, β is the learning rate update ratio, which is taken as 0.98 in this study, and the learning rate update interval is one cycle. When estimating rice LAI using the CNN model, the reflectance of the 12 bands involved in this study or all the vegetation indices calculated were first taken as the model inputs. Immediately after that, the variables with very high correlation were eliminated using correlation analysis, and the reflectance and vegetation indices of the remaining bands were utilized as the new model inputs for rice LAI estimation. Meanwhile, the same input variables were fed into the MLP model for accuracy comparison.

Data enhancement and regularization

Overfitting is a common problem throughout the deep learning field. Overlearning the details and noise of the training data by the model can lead to poor performance on the validation set [39]. The overfitting problem can be effectively mitigated by data augmentation and regularization. In this study, the original dataset was rotated 45°, 90°, and 135° to increase the diversity of the training data, and the model learned a wider range of features by expanding the dataset to reduce the dependence on specific samples. Meanwhile, the overfitting was reduced by limiting the complexity of the model using the Elastic Net regularization algorithm, which is a combination of Lasso regression (L_1 regularization) and ridge regression (L_2 regularization) [40, 41]. The computation of its loss function L_E is shown in Eq. (2).

$$L_E = L + \lambda_1 \sum_{i=1}^{n} |\omega_i| + \lambda_2 \sum_{i=1}^{n} \omega_i^2 \tag{2}$$

where L represents the original loss function, λ_1 and λ_2 represent the coefficients of the penalty terms of L_1 and L_2 regularization, respectively, and ω_i is the weight. L_1 regularization achieves feature selection and dimensionality reduction by making some weights zero to generate sparse solutions, and L_2 regularization helps to smooth out the weights to avoid overweighting, which improves the generalization ability of the model. Elastic Net regularization is a dynamic combination of the above two regularizations, which integrates the advantages of the two regularizations and reduces the disadvantages of the two

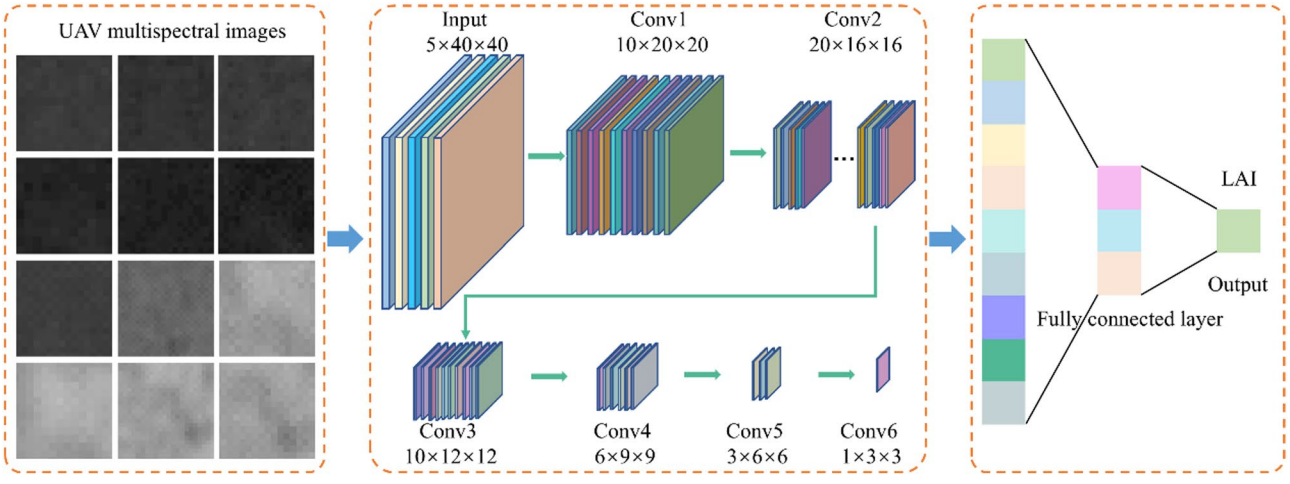

Fig. 4 The structural model of the CNN network

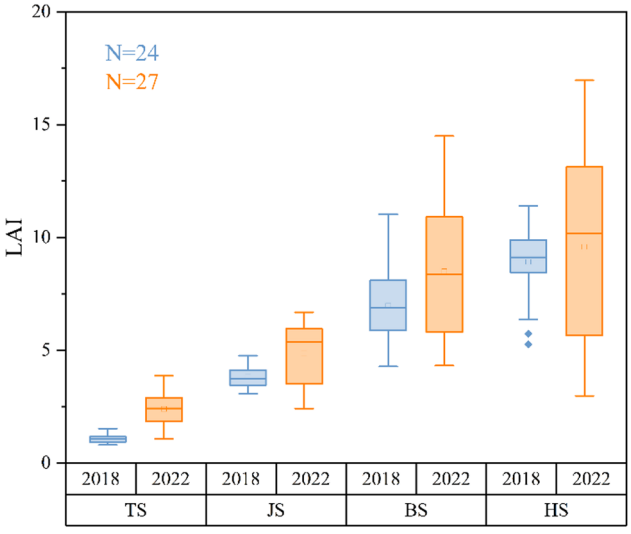

Fig. 5 Box plots of rice LAI changes at different periods

regularizations to a certain extent, and at the same time reduces the risk of model overfitting.

In this study, the data were collected from 51 sampling areas (27 in Trial 1 and 24 in Trial 2) at tillering stage (TS), jointing stage (JS), booting stage (BS), and heading stage (HS) of rice for model training and validation. The total number of samples was 204. The training and validation sets were randomly divided into 2:1. The coefficient of determination (R^2), Root mean square error (*RMSE*), and relative *RMSE* (*RRMSE*) were selected for accuracy statistics. Statistically, the larger the R^2 value, the smaller the *RMSE* and *RRMSE*, the higher the accuracy of the model, and the formulas for each accuracy index are as follows.

$$R^2 = 1 - \frac{\sum_{i=1}^{n}(y - \widehat{y})^2}{\sum_{i=1}^{n}(y - \overline{y})^2} \tag{3}$$

$$RMSE = \sqrt{\frac{\sum_{i=1}^{n}(\widehat{y} - y)^2}{n}} \tag{4}$$

$$RRMSE = \frac{RMSE}{\overline{y}} \tag{5}$$

where y, $\widehat{y}$, and $\overline{y}$ represent the measured, estimated, and mean of the measured values of rice LAI, respectively, and n is the number of samples.

In this study, several commonly used machine learning algorithms, including multivariate stepwise regression (MSR), support vector regression (SVR), and random forest regression (RFR), were used to compare their accuracy with that of deep learning models. Overall, the independent variables in this study can be categorized into reflectance and vegetation index. Before modeling, the independent variables were screened by correlation analysis. Overfitting was avoided by introducing data enhancement and regularization to improve the robustness of the models.

Results

Trends in LAI and canopy reflectance of rice at different periods

In the 2018 and 2022 experiments, the LAI variation trends and data distribution of rice at TS, JS, BS, and HS were analyzed and the results are shown in Fig. 5. It can be seen that the mean rice LAI values showed consistent trend of gradual increase over time in both experiments. The interquartile range revealed that the variability of LAI was smaller in the 2018 experiment and larger in the 2022 experiment, and maintained consistent LAI growth characteristics over the four periods. This is due to the inclusion of a japonica variety in the 2022 experiment, whereas the varieties in the 2018 experiment were all indica. Rice structure and morphology varied greatly between indica and japonica rice. To increase sample size and data complexity, data from both experiments were mixed for model training and validation for rice LAI estimation.

As an example, three plots in the 2022 experiment were used to exhibit changes in canopy reflectance of different rice varieties over four periods. In general, as can be seen from Fig. 6, the canopy reflectance demonstrated

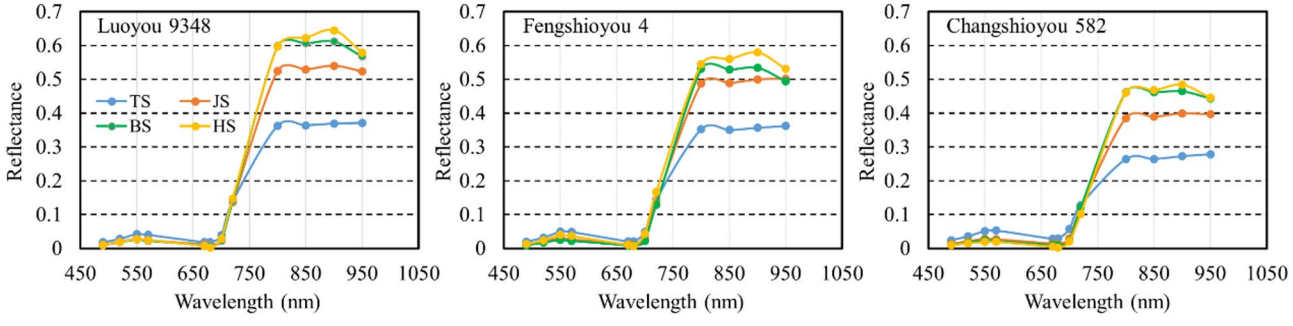

Fig. 6 Trends in canopy reflectance of rice at different periods

significant changes with the growth and development of rice. In the red edge to near-infrared wavelength bands (700–950 nm), the reflectance was the first to increase dramatically, and then the increase slowed down significantly. In the visible bands (490–680 nm), the reflectance first decreased gradually, and then the variation decreased. All three different rice varieties showed relatively consistent trends over time. Among the different varieties, Changshioyou 582 displayed an overall lower canopy reflectance during the same period, especially in the near-infrared bands.

Correlation analysis between vegetation indices and LAI at different periods

To screen the input variables for the multilayer perceptron, the correlation analysis was executed between rice LAI and the corresponding canopy vegetation indices for different periods. The correlations of the constructed twelve vegetation indices with single-period/multi-period rice LAI were evaluated using Pearson's correlation coefficient at a significance level of 0.05, and the results are shown in Fig. 7(a). It can be found that the performance of different vegetation indices correlated with single-period/multi-period rice LAI showed significant differences. At the tillering stage, all selected vegetation indices showed a high correlation with LAI except RVI and DVI. The correlation coefficients of OSAVI, SAVI, EVI2, MTCI, and NDRE with LAI were greater than 0.7. At the jointing stage, the correlation coefficients of all the vegetation indices with LAI were more than 0.4 but less than 0.7. The vegetation indices with a strong correlation with the LAI of rice behaved similarly to the tillering stage. The correlation coefficients of vegetation indices with LAI generally weakened at the booting stage compared to the previous two periods, with only OSAVI, SAVI, and RVI having correlation coefficients with LAI exceeding 0.6. At the heading stage, the correlation between vegetation indices and LAI further weakened. The correlation coefficients between vegetation indices and LAI for all the selected vegetation indices except RVI were less than 0.6. Most of the vegetation indices had a strong correlation with LAI from multiple periods. In particular, the correlation coefficients of OSAVI, WDRVI, SAVI, RVI, EVI2, EVI, and NDRE with LAI were more than 0.6.

The seven vegetation indices mentioned above were initially identified as input variables for the multilayer perceptron. To avoid information redundancy caused by the input of strongly linearly correlated variables, the correlations between different vegetation indices were analyzed and the results are shown in Fig. 7(b). It can be observed that among the initially identified input variables, OSAVI was strongly correlated with SAVI and EVI, and WDRVI was strongly correlated with EVI2. Therefore, after removing the strongly correlated variables, OSAVI, RVI, EVI2, and NDRE were finally identified as input variables for estimating rice LAI by the multilayer perceptron model.

Screening of input variables for the CNN model at different periods

Like the way of determining the input variables for the MLP model, the weakly correlated bands were filtered out as the inputs to the CNN model by analyzing the

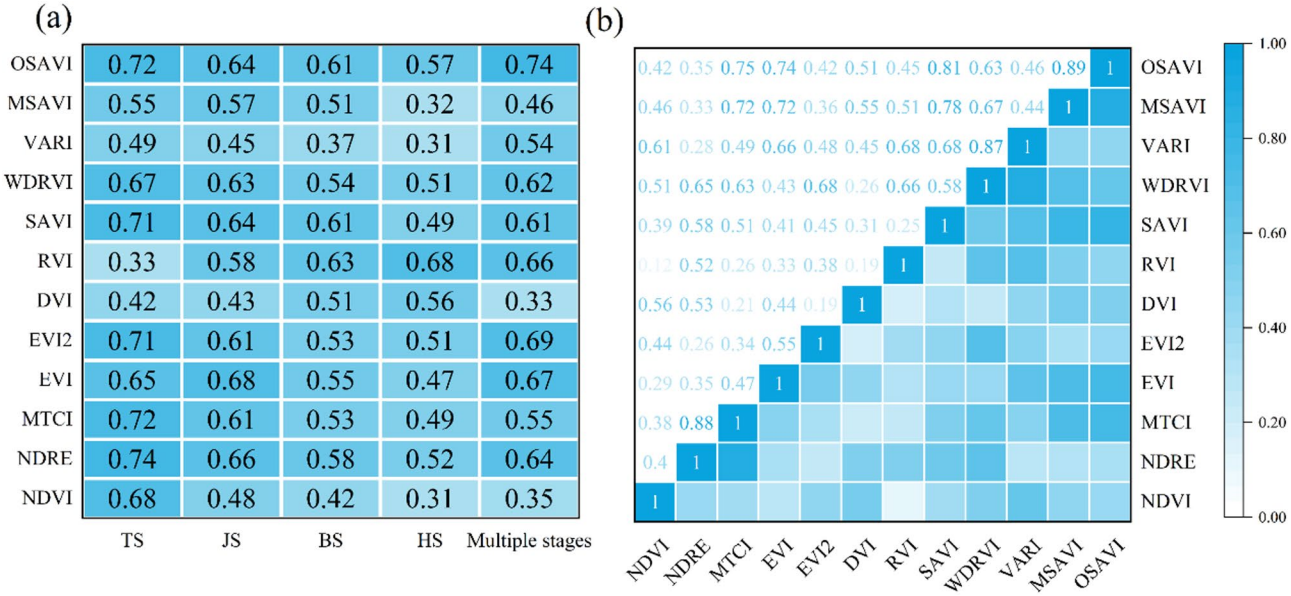

Fig. 7 Heat maps of the correlation: (**a**) the Pearson correlation coefficients between rice canopy vegetation indices and LAI; (**b**) the correlation between vegetation indices

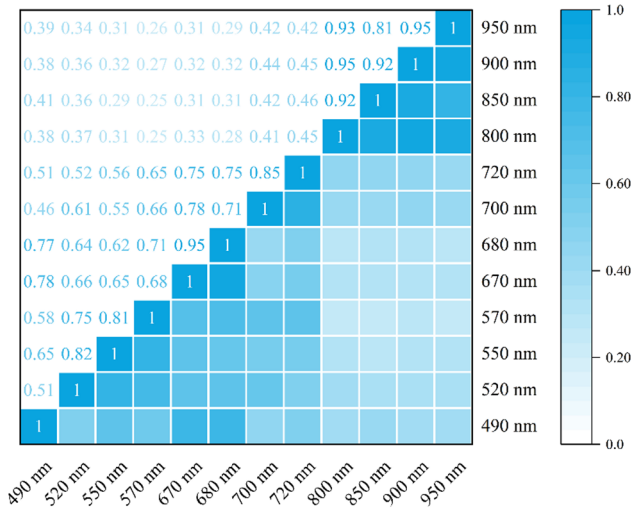

Fig. 8 The correlation between the reflectance of different bands

correlation between the reflectance of different bands and removing the highly correlated variables. Figure 8 illustrates the correlation between the reflectance of different bands for multiple periods. It was observed that there was a strong correlation between the reflectance of the bands 490, 670, and 680 nm, 520, 550, and 570 nm, 570, 670, 680, and 700 nm, 700 and 720 nm, as well as the bands 800, 850, 900, and 950 nm. Furthermore, it was considered that the commonly used multispectral bands were composed of blue, green, red, red-edge, and near-infrared bands. The finalized CNN input variables in this study were the reflectance images of 490,550,670,720,850 nm.

Rice LAI Estimation based on the MLP and CNN

In this study, the estimation models of rice LAI at different periods were constructed using OSAVI, RVI, EVI2, and NDRE as inputs to the MLP network model. Meanwhile, a CNN-based model for estimating the LAI of rice at a single period was constructed using reflectance images at 490,550,670,720,850 nm bands as inputs. The results of estimating single-period rice LAI using MLP and CNN models are shown in Fig. 9. It was found that the accuracy of rice LAI estimation gradually decreased over time in the MLP-based estimation results. There is a large difference between the accuracy of the training set and the validation set. During the booting and heading periods, the data points in the validation set deviated significantly from the 1:1 line, and there was an obvious underestimation phenomenon. In the CNN-based estimation results, the difference in accuracy between the training and validation sets was significantly reduced. The trend of rice LAI estimation accuracy over time was generally consistent with that of the MLP model. During the heading period, the model accuracy was significantly lower than that of the previous periods. However, the phenomenon of model underestimation was substantially improved. Overall, the estimation accuracy of the CNN-based model was significantly higher than that of the MLP model. Compared with the MLP model, the accuracy of rice LAI estimation based on the CNN model

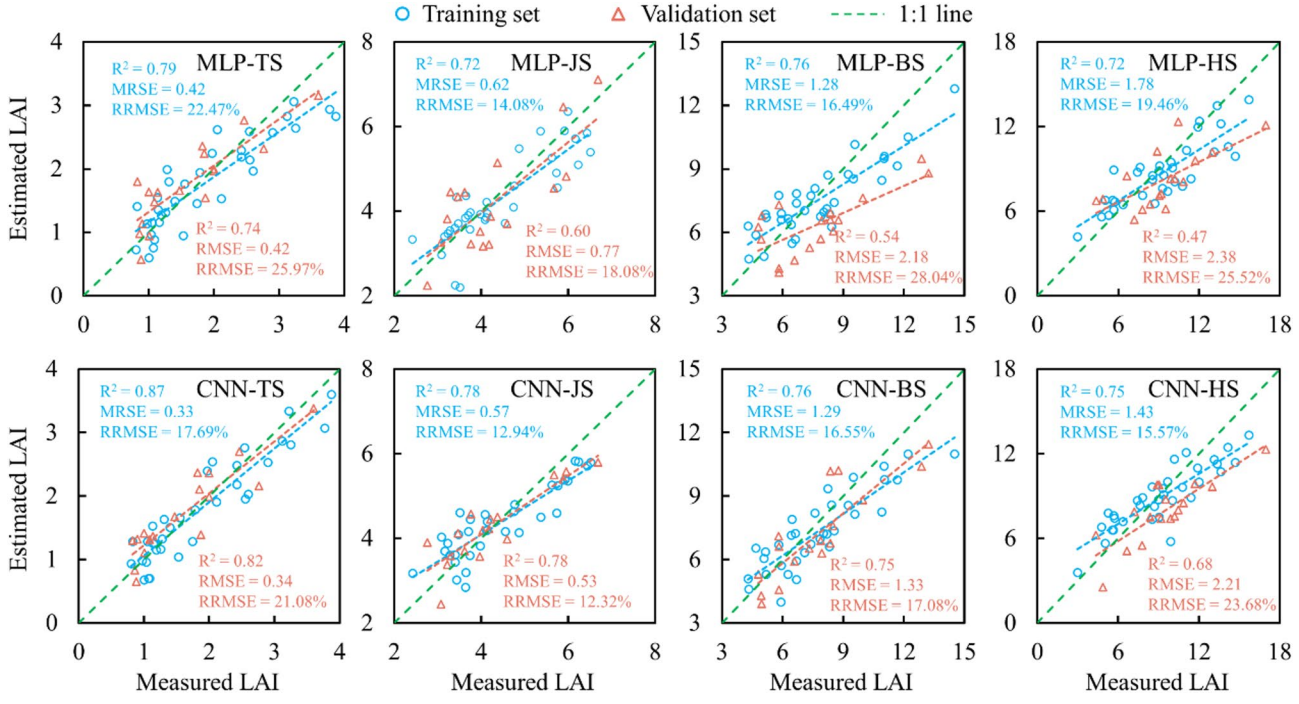

Fig. 9 The accuracy comparison of single-period rice LAI estimation based on MLP and CNN

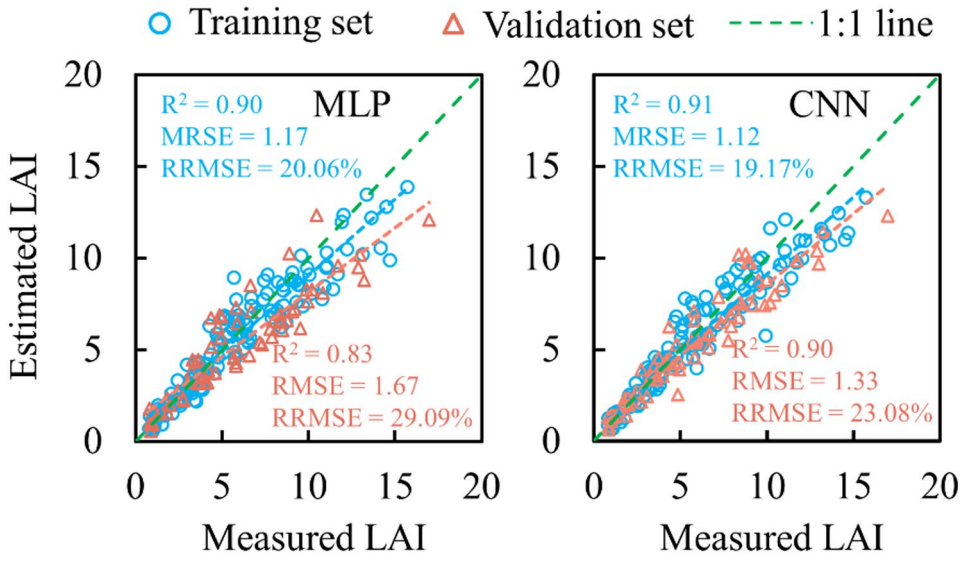

Fig. 10 The accuracy comparison of multi-period rice LAI estimation based on MLP and CNN

Table 2 The accuracy comparison of deep learning and machine learning models for estimating rice LAI over multiple periods with different variable inputs

Input variable combination	Training set			Validation set		
	R^2	RMSE	RRMSE	R^2	RMSE	RRMSE
All vegetation indices-MLP	0.88	1.28	22.03%	0.81	1.80	31.26%
Reflectance of all bands-MLP	0.91	1.16	20.01%	0.73	2.10	36.55%
All vegetation indices-CNN	0.92	1.15	19.78%	0.84	1.64	28.45%
Vegetation indices screening-CNN	0.89	1.23	21.15%	0.86	1.53	26.62%
Vegetation indices screening-MSR	0.81	1.86	32.01%	0.66	2.86	49.78%
Vegetation indices screening-SVR	0.82	1.78	30.63%	0.71	1.94	33.71%
Vegetation indices screening-RFR	0.85	1.58	27.21%	0.74	1.91	33.15%

was improved by 0.08, 0.18, 0.21, 0.21 for R^2, reduced by 0.08, 0.24, 0.85, 0.17 for RMSE, and reduced by 4.89, 5.76, 10.96, 1.84% for RRMSE at TS, JS, BS and HS, respectively.

The results of estimating rice LAI for multiple periods using MLP and CNN models are shown in Fig. 10. It can be seen that there was a large difference in model accuracy between the training and validation sets when utilizing MLP, with a difference of 0.07 in R^2, 0.5 in RMSE, and 9.03% in RRMSE. The fitting line of the validation set deviated far from the 1:1 line, with a significant underestimation. When CNN was utilized, the difference in model accuracy between the training and validation sets was significantly reduced, with a difference of 0.01 in R^2, 0.21 in RMSE, and 3.91% in RRMSE. The accuracy of the validation set was $R^2 = 0.90$, RMSE = 1.33, and RRMSE = 23.08%. The model generalization ability was enhanced and the underestimation was improved. Compared with the MLP model, the accuracy of the CNN-based model for estimating rice multi-period LAI was improved by 0.07 in R^2, reduced by 0.34 in RMSE, and reduced by 6.01% in RRMSE, respectively.

To further illustrate the effect of input variable selection on model accuracy, all constructed variables were used as model inputs when utilizing MLP and CNN, and the results were compared with the screened variable inputs. The effects of vegetation index and reflectance inputs on model accuracy were also compared by variable swapping. The results of the above comparison are shown in Table 2. The results showed that when all constructed vegetation indices were input into the MLP, the accuracy of LAI estimation was reduced by 2.17% compared with the screened vegetation index input results. The model accuracy was reduced by 7.46% when using all reflectance as MLP input. This suggested that the vegetation index could better reflect the rice LAI changes compared to the reflectance when utilizing MLP. When all constructed vegetation index images were input into the CNN, the LAI estimation accuracy was reduced by 4.65% compared to the filtered reflectance image input results. When the screened vegetation index images were input into the CNN, the rice LAI estimation accuracy was reduced by 3.54% compared with the screened reflectance image input results. The above results indicated

that for different deep learning models, varying input variable types as well as variable screening had a greater impact on the model accuracy. Model redundancy would reduce the model accuracy of deep learning.

To rigorously evaluate the comparative advantages of deep learning in rice LAI estimation, we conducted a systematic benchmark analysis against conventional machine learning algorithms. As demonstrated in Table 2, traditional machine learning approaches exhibited generally inferior estimation accuracy compared to deep learning architectures, with relative performance differences exceeding 14% in RRMSE metrics. Notably, the RFR algorithm achieved marginally superior performance (R^2 = 0.74 vs. 0.73) over the MLP model utilizing reflectance of all bands, potentially attributable to its inherent robustness in handling high-dimensional spectral collinearity.

The results in Table 2 conclusively showed that the accuracy of deep learning models was generally higher than that of machine learning in rice LAI estimation. The accuracy of the models after variable screening was significantly higher than that of the models with all variables directly input. This fully illustrated the importance of variable screening combined with deep learning in regression prediction.

Discussion

Effects of the input variable types on the accuracy of deep learning models for estimating LAI in rice

Reflectance and vegetation indices, as simple and easily accessible spectral information, are often used as input variables for deep-learning models to estimate crop growth information and yield. Most current studies rely on the utilization of vegetation indices to build LAI estimation models [15, 42]. When manually extracting feature variables, much effective information was frequently lost resulting in limited model accuracy. In recent years, artificial intelligence has developed rapidly, and deep neural networks and convolutional neural networks have made great progress in estimating crop growth parameters [43, 44]. Multivariate fusion prediction models based on multilayer perceptron networks are widely applied to vegetation monitoring and parameter inversion [45, 46]. The application of CNN avoids feature loss caused by manual extraction and provides an alternative method to automatically learn rich features from large raw image datasets [47]. Remotely sensed spectral data combined with deep learning can be used for rice LAI estimation, but fewer studies directly use raw multispectral images as input to CNN models. In most of the existing studies on crop LAI estimation using canopy reflectance, the extracted reflectance or textual information of reflectance transformation was used as the model independent variables, and the reflectance image information was not sufficiently mined. For example, feature parameters such as the first-order derivative [48], the envelope removal [49], and the wavelet transform [50] are widely utilized to enhance the accuracy of crop LAI estimation.

Spectral saturation in densely vegetated areas is one of the major problems faced by the remote sensing community [51], which hinders the application of broadband remote sensing data and its derivatives in vegetation monitoring [52]. This severely limits the accuracy of most current inversion models based on vegetation indices. When the canopy completely covers off the soil in the middle and late stages of rice growth, the change of the canopy vegetation index with time is no longer obvious. Canopy images of typical vegetation indices at different periods are presented in Fig. 11. It can be seen that after the rice jointing stage, the canopy is gradually closed and NDVI, NDRE, and OSAVI all show different degrees of saturation. This directly resulted in a gradual decrease in the correlation between vegetation index and LAI (Fig. 7a). The phenomenon is also more common in other studies of growth parameter estimation. For example, the same problem of spectral vegetation index saturation was encountered in estimating soybean biomass using vegetation index combined with machine learning [53]. There is currently no standard procedure in the remote sensing community to solve the spectral saturation problem [52].

It will be difficult to reflect the growth of the canopy when the vegetation index is saturated, but the typical characteristics of crop growth will be reflected in the original image. For example, the growth of spikes at the rice heading stage can be a new effective feature, which is difficult to recognize by traditional methods. Moreover, spectral reflectance can show more vegetation-background details. The changing characteristics of reflectance images of different bands at different periods are illustrated in Fig. 12. It can be observed that the reflectance images do not produce significant saturation compared with the vegetation index map. For many leaves, information such as rice spikes can still be clearly displayed. Furthermore, the information displayed in different bands is not the same, showing rich canopy information. The use of CNN to establish a rice LAI estimation model can maximize the use of the original image information and overcome the related problems, thus producing higher LAI estimation accuracy (Figs. 9 and 10). In future studies, the spatial features obtained from image transformations can be fully utilized to further improve the accuracy of rice LAI estimation, such as Fourier transform and wavelet transform [54, 55].

Adaptation of LAI Estimation models over time

There are significant differences in the physiological and morphological characteristics of rice at different growth stages [56]. The variations in growth stages will change

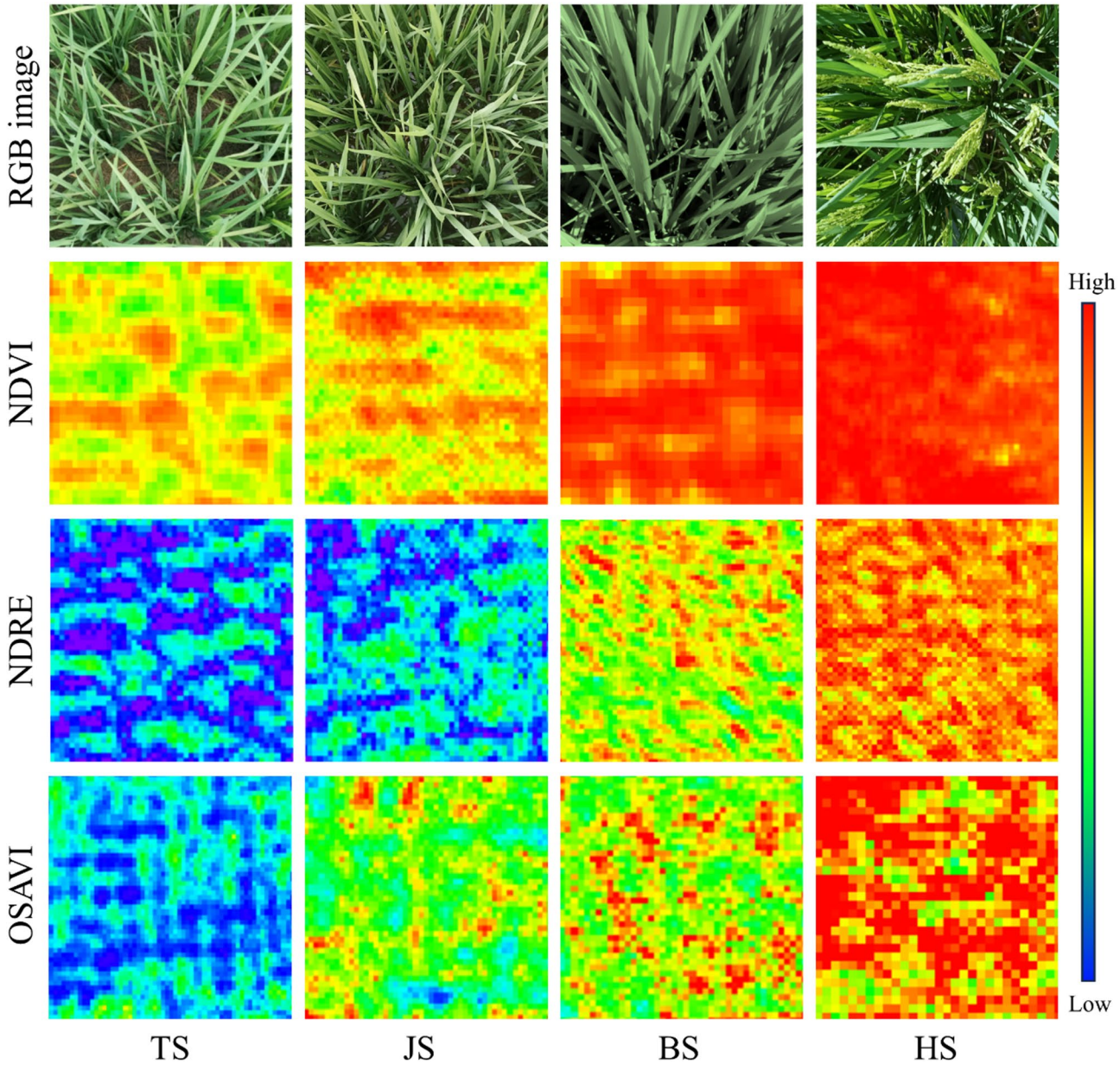

Fig. 11 The images comparison of vegetation indices at different periods

the vegetation structure, canopy cover, and optical characteristics, which will have a greater impact on the accuracy of the inversion models [57]. In existing studies, the general process adopted is to establish the regression relationship between the characteristic variables and the measured data for the whole period or multiple periods to ensure the high accuracy of the overall model while ignoring the availability of a single period [58]. The description and assessment of model applicability at different growth stages of crops are lacking in most existing studies. In this study, rice LAI prediction models for four rice key growth stages, TS, JS, BS, and HS, were developed and evaluated for accuracy. The results in Fig. 9 show that the CNN model based on multiple bands of reflectance as inputs exhibits more satisfactory prediction accuracy at all stages. Compared to the multilayer perceptron model with vegetation indices as inputs, the rice LAI prediction accuracy was improved by 4.89, 5.76, 10.96, and 1.84%, respectively, over the four periods of observation. Few existing studies have evaluated the estimation accuracy of rice LAI based on different individual periods. Accuracy improvement over multiple periods is the main objective in most studies [59]. In addition, more studies focused on soil background removal and the effect of rice spikes [54, 60, 61]. Some image processing techniques can indeed improve the accuracy of rice

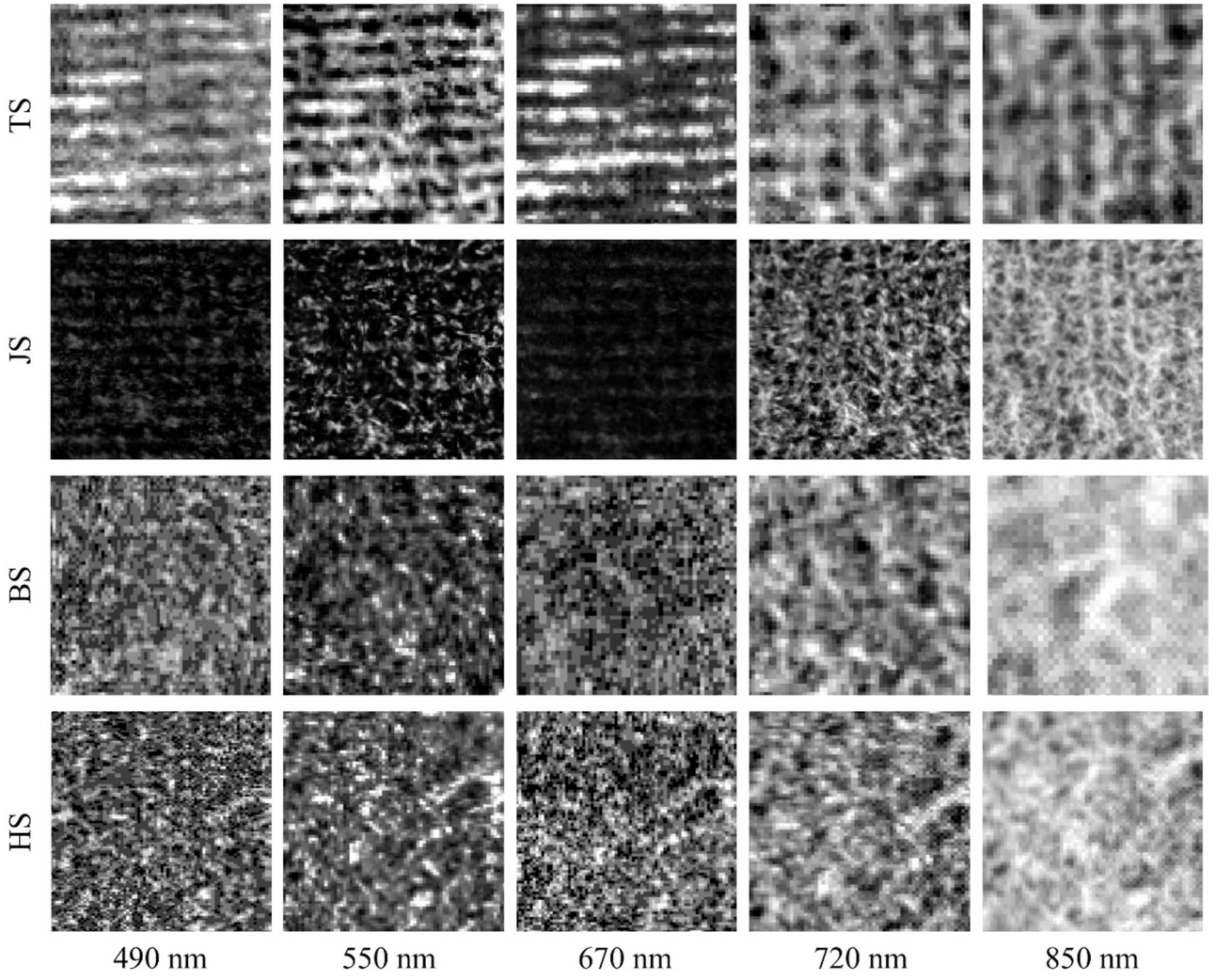

Fig. 12 The image comparison of reflectance at different periods

LAI estimation, but the process is relatively complicated. In this study, rice LAI estimation is directly based on the original canopy reflectance data, which simplifies the operation process.

Data enhancement and regularization were used in this study to mitigate the overfitting problem of the model. Feature enhancement was achieved by rotating the images. In deep learning, models need to make correct predictions by learning key features in the data [62]. When the image is rotated for enhancement, the important features of the image may be altered, and the rotation operation may make it difficult to capture the key features, which may affect the performance of the model [63]. However, after rotating through multiple angles, the model's dependence on specific samples can be reduced to enhance adaptation over multiple periods. In addition, the risk of model overfitting was reduced by the Elastic Net regularization algorithm. Data enhancement combined with regularization achieved the generalization of the CNN model to predict LAI over multiple periods.

The effects of variable screening on the accuracy of deep learning models for estimating LAI in rice

Variable screening is frequently overlooked when using machine learning and deep learning regression prediction. Multiple types or multiple variables are considered equally important and are directly input into the model. For example, in rice LAI prediction, multiple vegetation indices and texture parameters were input into multiple linear regression and random forest models to obtain more accurate results than using only spectral information [18]. Although the importance of the different variables was compared, covariates or irrelevant variables were not eliminated. In potato biomass and yield prediction, the reflectance of all bands of the hyperspectral data was input into the PLSR and RF models, ignoring the

effects of band redundancy and noise in the hyperspectral data [17]. In this study, deep learning models based on different types and different numbers of variables as inputs were compared (Table 2). The results showed that the model accuracy was not the highest when all variables were served as model inputs. In the MLP model, OSAVI, RVI, EVI2, and NDRE had the highest model accuracy when they were used as inputs. In the CNN models, the best model accuracy was obtained when based on the reflectance images of 490,550,670,720,850 nm bands as inputs. The model accuracy was limited when using other types and unscreened variable inputs. The above results fully demonstrated the significant role of variable screening for LAI estimation in rice. It also indicated the good adaptability of the CNN model in multiple rice periods.

The findings of this study suggest that variable screening can eliminate irrelevant or redundant features and retain those that are most useful for model prediction. In deep learning models, the covariance between variables may lead to degradation of model performance. Through variable screening, the covariance between features can be reduced to improve the stability and prediction ability of the model. Additionally, variable screening helps to reduce the complexity of the model and improve the computational efficiency. Existing studies have shown that variable screening can contribute to the construction of a more concise and effective model structure and improve the interpretability of the model [64]. Through variable screening, overfitting can be avoided and the generalization ability of the model on unknown data can be improved.

In future studies, feature screening methods such as principal component analysis, RRelief, and machine learning will be further used to optimize the variable screening process [17, 65]. In this study, five bands of spectral reflectance images were used as model inputs, assuming the premise that each band has the same weight of influence on the prediction results. This assumption may limit the accuracy and stability of the model. Therefore, the importance or weighting of the input variables deserves to be considered.

Of course, some other factors may have effects on the results of this experiment. First, the quality of the multispectral reflectance data may significantly affect the modeling results. The accuracy of the reflectance data is highly dependent on the radiometric calibration [30]. In this study, the PEL method has been shown to work well in acquiring both lower and higher reflectances. Secondly, data acquisition conditions can also affect the accuracy of rice LAI estimation. For example, there will be variability in reflectance data acquired at different heights, angles, and times [30]. Such effects of spatial and temporal scales were not explored in this study. The extent of its influence on LAI estimation needs to be further explored in the follow-up. Finally, in the modeling process, the size of data samples and the setting of model parameters can have a significant impact on the model accuracy [66]. In this study, the Adam optimizer was used to determine the model parameters. The data sample size aspect may not have been addressed and should be taken into consideration for future studies.

Conclusions

This study established a unified multi-temporal estimation framework for rice canopy LAI by integrating UAV-derived multispectral imagery with deep learning architectures. Comparative analysis of MLP and CNN models revealed that the CNN-based approach demonstrated superior performance in LAI estimation (validation set: R^2 = 0.90, RMSE = 1.33, RRMSE = 23.08%). The CNN architecture effectively leveraged raw multispectral reflectance data through automated hierarchical feature extraction, circumventing the spectral saturation limitations inherent in traditional VI-based methods, particularly in dense vegetation canopies. Furthermore, the CNN exhibited enhanced temporal adaptability by capturing dynamic physiological and morphological variations across distinct growth stages, thereby achieving robust cross-phenological LAI predictions. Moverover, input variable optimization emerged as a critical determinant of model efficacy. Strategic selection of spectral reflectance bands and vegetation indices substantially improved estimation accuracy while mitigating overfitting risks. The integration of data augmentation and regularization techniques further enhanced model generalizability across multi-temporal datasets. These findings underscore the necessity of preserving raw spectral information while implementing systematic feature engineering and model calibration protocols for remote sensing-driven deep learning applications. The proposed UAV-CNN framework provides a scalable and precise solution for multi-temporal LAI monitoring in rice cultivation systems. This study has several noteworthy limitations. First, the experimental protocol was confined to a limited number of rice cultivars under artificially managed cultivation environments. Furthermore, the absence of validation using canopy spectral data from heterogeneous field environments with uncontrolled variables (e.g., natural pest pressures, unregulated nutrient gradients, and spontaneous weed competition) restricts definitive conclusions about the model's agroecological adaptability. This constrained scope may affect the generalizability of the proposed framework across diverse farming systems and genotypes. Future research should focus on three directions: (1) exploration of more variable screening methods; (2) cross-species validation to assess broader applicability in gramineous crop monitoring; (3)

architectural refinements using hybrid neural networks to exploit spatial-spectral-temporal correlations.

Acknowledgements
We thank all the members from Laboratory 301, School of Remote Sensing and Information Engineering, Wuhan University.

Author contributions
HL and SL designed the experiments. QL and SL performed the experiments. HL and CY analyzed the data and wrote this manuscript. SL checked the language.

Funding
The research presented in this paper was funded by Joint Fund of Henan Province Science and Technology R&D Program (235200810069), Science and Technology Tackling Project of Henan Province (242102210011, 242102210069), Basic Research Operating Expenses Program of Henan Academy of Sciences (240625002), and Scientific Research Initiation Program for High-level Talents of Henan Academy of Sciences (241825015).

Data availability
No datasets were generated or analysed during the current study.

Declarations

Ethics approval and consent to participate
Not applicable.

Consent for publication
Not applicable.

Competing interests
The authors declare no competing interests.

Received: 10 March 2025 / Accepted: 22 May 2025
Published online: 30 May 2025

References

1. Zhu Y, Su H, Liu XX, Sun JF, Xiang L, Liu YJ, et al. Identification of NADPH oxidase genes crucial for rice multiple disease resistance and yield traits. Rice. 2024;17:15.
2. Chen C, Bao YX, Zhu F, Yang RM. Remote sensing monitoring of rice growth under Cnaphalocrocis Medinalis (Guenée) damage by integrating satellite and UAV remote sensing data. Int J Remote Sens. 2024;45:772–90.
3. Hashim N, Ali MM, Mahadi MR, Abdullah AF, Wayayok A, Kassim MSM, et al. Smart farming for sustainable rice production: an insight into application, challenge, and future prospect. Rice Sci. 2024;31:47–61.
4. Chen L, Deng XY, Duan HX, Tan XM, Xie XB, Pan XH, et al. Canopy humidity and irrigation regimes interactively affect rice physiology, grain filling and yield during grain filling period. Agric Water Manage. 2025;307:10.
5. Wu TZ, Zhang ZW, Wang Q, Jin WJ, Meng K, Wang C, et al. Estimating rice leaf area index at multiple growth stages with Sentinel-2 data: an evaluation of different retrieval algorithms. Eur J Agron. 2024;161:17.
6. Li CM, Teng X, Tan Y, Zhang Y, Zhang HC, Xiao D, et al. Spatio-temporal mapping of leaf area index in rice: spectral indices and multi-scale texture comparison derived from different sensors. Front Plant Sci. 2024;15:15.
7. Liu TJ, Duan SB, Liu NT, Wei B, Yang JT, Chen JK, et al. Estimation of crop leaf area index based on Sentinel-2 images and PROSAIL-Transformer coupling model. Comput Electron Agric. 2024;227:18.
8. Liu XY, He L, He ZW, Wei Y. Estimation of forest leaf area index based on GEE data fusion method. IEEE J Sel Top Appl Earth Observ Remote Sens. 2025;18:4510–24.
9. Luo SZ, Liu WW, Ren Q, Wei HQ, Wang C, Xi XH, et al. Leaf area index Estimation in maize and soybean using UAV lidar data. Precis Agric. 2024;25:1915–32.
10. Tian XC, Jia XY, Da Y, Liu JY, Ge WY. Evaluating the sensitivity of vegetation indices to leaf area index variability at individual tree level using multispectral drone acquisitions. Agric Meteorol. 2025;364:11.
11. Cheng ZQ, Chen JM, Guo ZX, Miao GF, Zeng HD, Wang R, et al. Improving UAV-Based LAI Estimation for forests over complex terrain by reducing topographic effects on multispectral reflectance. IEEE Trans Geosci Remote Sens. 2024;62:19.
12. Ingalls TC, Li JW, Sawall Y, Martin RE, Thompson DR, Asner GP. Imaging spectroscopy investigations in wet carbon ecosystems: A review of the literature from 1995 to 2022 and future directions. Remote Sens Environ. 2024;305:23.
13. Verhoef W. Light-scattering by leaf layers with application to canopy reflectance modeling - the SAIL model. Remote Sens Environ. 1984;16:125–41.
14. Wang Q, Sun DY, Li YM, Le CF, Huang CC. Mechanisms of remote-sensing reflectance variability and its relation to bio-optical processes in a highly turbid eutrophic lake: lake Taihu (China). IEEE Trans Geosci Remote Sens. 2010;48:575–84.
15. Chatterjee S, Baath GS, Sapkota BR, Flynn KC, Smith DR. Enhancing LAI Estimation using multispectral imagery and machine learning: A comparison between reflectance-based and vegetation indices-based approaches. Comput Electron Agric. 2025;230:13.
16. Jay S, Maupas F, Bendoula R, Gorretta N. Retrieving LAI, chlorophyll and nitrogen contents in sugar beet crops from multi-angular optical remote sensing: comparison of vegetation indices and PROSAIL inversion for field phenotyping. Field Crop Res. 2017;210:33–46.
17. Li B, Xu XM, Zhang L, Han JW, Bian CS, Li GC, et al. Above-ground biomass Estimation and yield prediction in potato by using UAV-based RGB and hyperspectral imaging. ISPRS-J Photogramm Remote Sens. 2020;162:161–72.
18. Li SY, Yuan F, Ata-Ui-Karim ST, Zheng HB, Cheng T, Liu XJ, et al. Combining color indices and textures of UAV-Based digital imagery for rice LAI Estimation. Remote Sens. 2019;11:21.
19. Maimaitijiang M, Sagan V, Sidike P, Hartling S, Esposito F, Fritschi FB. Soybean yield prediction from UAV using multimodal data fusion and deep learning. Remote Sens Environ. 2020;237:20.
20. Roosjen PPJ, Brede B, Suomalainen JM, Bartholomeus HM, Kooistra L, Clevers J. Improved Estimation of leaf area index and leaf chlorophyll content of a potato crop using multi-angle spectral data - potential of unmanned aerial vehicle imagery. Int J Appl Earth Obs Geoinf. 2018;66:14–26.
21. Richter K, Atzberger C, Vuolo F, Weihs P, D'Urso G. Experimental assessment of the Sentinel-2 band setting for RTM-based LAI retrieval of sugar beet and maize. Can J Remote Sens. 2009;35:230–47.
22. Xu XQ, Lu JS, Zhang N, Yang TC, He JY, Yao X, et al. Inversion of rice canopy chlorophyll content and leaf area index based on coupling of radiative transfer and bayesian network models. ISPRS-J Photogramm Remote Sens. 2019;150:185–96.
23. Esmaeili M, Abbasi-Moghadam D, Sharifi A, Tariq A, Li QT. ResMorCNN model: hyperspectral images classification using Residual-Injection morphological features and 3DCNN layers. IEEE J Sel Top Appl Earth Observ Remote Sens. 2024;17:219–43.
24. Akhtarmanesh A, Abbasi-Moghadam D, Sharifi A, Yadkouri MH, Tariq A, Lu LL. Road extraction from satellite images using Attention-Assisted UNet. IEEE J Sel Top Appl Earth Observ Remote Sens. 2024;17:1126–36.
25. Mahdipour H, Sharifi A, Sookhak M, Medrano CR, Ultrafusion. Optimal fuzzy fusion in Land-Cover segmentation using multiple panchromatic satellite images. IEEE J Sel Top Appl Earth Observ Remote Sens. 2024;17:5721–33.
26. Vafaeinejad A, Alimohammadi N, Sharifi A, Safari MM, Super-Resolution. AI-Based approach for extracting agricultural cadastral maps: form and content validation. IEEE J Sel Top Appl Earth Observ Remote Sens. 2025;18:5204–16.
27. Nejad SMM, Abbasi-Moghadam D, Sharifi A. ConvLSTM-ViT: A deep neural network for crop yield prediction using Earth observations and remotely sensed data. IEEE J Sel Top Appl Earth Observ Remote Sens. 2024;17:17489–502.
28. Deng L, Hao XL, Mao ZH, Yan YN, Sun J, Zhang AW. A subband radiometric calibration method for UAV-based multispectral remote sensing. IEEE J Sel Top Appl Earth Observ Remote Sens. 2018;11:2869–80.
29. Deng L, Mao ZH, Li XJ, Hu ZW, Duan FZ, Yan YN. UAV-based multispectral remote sensing for precision agriculture: A comparison between different cameras. ISPRS-J Photogramm Remote Sens. 2018;146:124–36.
30. Luo SJ, Jiang XQ, Yang KL, Li YJ, Fang SH. Multispectral remote sensing for accurate acquisition of rice phenotypes: impacts of radiometric calibration and unmanned aerial vehicle flying altitudes. Front Plant Sci. 2022;13:19.
31. Richardson AJ, Wiegand C. Distinguishing vegetation from soil background information. Photogram Eng Remote Sens. 1977;43:1541–52.
32. Jordan CF. Derivation of leaf area index from light quality of the forest floor. Ecology. 1969;50:663–6.

33. Rouse JW, Haas RH, Schell JA, Deering DW. Monitoring vegetation systems in the great plains with ERTS. NASA Special Publication. 1974;351.
34. Gitelson A, Merzlyak MN. Quantitative Estimation of chlorophyll-a using reflectance spectra - experiments with autumn chestnut and maple leaves. J Photochem Photobiol B-Biol. 1994;22:247–52.
35. Gitelson AA, Kaufman YJ, Stark R, Rundquist D. Novel algorithms for remote Estimation of vegetation fraction. Remote Sens Environ. 2002;80:76–87.
36. Jiang ZY, Huete AR, Didan K, Miura T. Development of a two-band enhanced vegetation index without a blue band. Remote Sens Environ. 2008;112:3833–45.
37. Gitelson AA. Wide dynamic range vegetation index for remote quantification of biophysical characteristics of vegetation. J Plant Physiol. 2004;161:165–73.
38. Khalifani S, Darvishzadeh R, Azad N, Rahmani RS. Prediction of sunflower grain yield under normal and salinity stress by RBF, MLP and, CNN models. Ind Crop Prod. 2022;189:11.
39. Xiong HT, Li J, Wang TW, Zhang F, Wang ZY. EResNet-SVM: an overfitting-relieved deep learning model for recognition of plant diseases and pests. J Sci Food Agric. 2024;104:6018–34.
40. Bedoui A, Lazar NA. Bayesian empirical likelihood for ridge and Lasso regressions. Comput Stat Data Anal. 2020;145:15.
41. Choi SH, Jung HY, Kim H. Ridge fuzzy regression model. Int J Fuzzy Syst. 2019;21:2077–90.
42. Wei SS, Yin TG, Yuan B, Lim KH, Liew SC, Whittle AJ. Optimizing UAV hyperspectral imaging for urban tree chlorophyll and leaf area index retrieval. IEEE J Sel Top Appl Earth Observ Remote Sens. 2025;18:839–52.
43. Zhou HK, Huang FD, Lou WD, Gu Q, Ye ZR, Hu H, et al. Yield prediction through UAV-based multispectral imaging and deep learning in rice breeding trials. Agric Syst. 2025;223:15.
44. Yamaguchi T, Takamura T, Tanaka TST, Ookawa T, Katsura K. A study on optimal input images for rice yield prediction models using CNN with UAV imagery and its reasoning using explainable AI. Eur J Agron. 2025;164:12.
45. Yue JB, Yang GJ, Li CC, Liu Y, Wang J, Guo W, et al. Analyzing winter-wheat biochemical traits using hyperspectral remote sensing and deep learning. Comput Electron Agric. 2024;222:17.
46. Cheng ZK, Gu XB, Du YD, Wei CY, Xu Y, Zhou ZH, et al. Multi-modal fusion and multi-task deep learning for monitoring the growth of film-mulched winter wheat. Precis Agric. 2024;25:1933–57.
47. Zhang CS, Yi Y, Wang LJ, Chen S, Li P, Zhang SX, et al. Efficient physics-informed transfer learning to quantify biochemical traits of winter wheat from UAV multispectral imagery. Smart Agric Technol. 2024;9:13.
48. Köksal ES. Agric Water Manage. 2011;98:1317–28. Hyperspectral reflectance data processing through cluster and principal component analysis for estimating irrigation and yield related indicators.
49. Luo SJ, He YB, Wang ZZ, Duan DD, Zhang JK, Zhang YT, et al. Comparison of the retrieving precision of potato leaf area index derived from several vegetation indices and spectral parameters of the continuum removal method. Eur J Remote Sens. 2019;52:155–68.
50. Zhang Y, Wang PX, Tansey K, Han D, Chen C, Liu JM, et al. Enhanced feature extraction from assimilated VTCI and LAI with a particle filter for wheat yield Estimation using Cross-Wavelet transform. IEEE J Sel Top Appl Earth Observ Remote Sens. 2023;16:5115–27.
51. Mutanga O, Adam E, Cho MA. High density biomass Estimation for wetland vegetation using WorldView-2 imagery and random forest regression algorithm. Int J Appl Earth Obs Geoinf. 2012;18:399–406.
52. Mutanga O, Masenyama A, Sibanda M. Spectral saturation in the remote sensing of high-density vegetation traits: A systematic review of progress, challenges, and prospects. ISPRS-J Photogramm Remote Sens. 2023;198:297–309.
53. Maimaitijiang M, Sagan V, Sidike P, Maimaitiyiming M, Hartling S, Peterson KT, et al. Vegetation index weighted canopy volume model (CVM < sub > VI) for soybean biomass Estimation from unmanned aerial System-based RGB imagery. ISPRS-J Photogramm Remote Sens. 2019;151:27–41.
54. Zhou C, Gong Y, Fang SH, Yang KL, Peng Y, Wu XT, et al. Combining spectral and wavelet texture features for unmanned aerial vehicles remote Estimation of rice leaf area index. Front Plant Sci. 2022;13:17.
55. Duan B, Liu YT, Gong Y, Peng Y, Wu XT, Zhu RS, et al. Remote Estimation of rice LAI based on fourier spectrum texture from UAV image. Plant Methods. 2019;15:12.
56. Zhou X, Zheng HB, Xu XQ, He JY, Ge XK, Yao X, et al. Predicting grain yield in rice using multi-temporal vegetation indices from UAV-based multispectral and digital imagery. ISPRS-J Photogramm Remote Sens. 2017;130:246–55.
57. Su X, Wang JC, Ding L, Lu JS, Zhang JW, Yao X, et al. Grain yield prediction using multi-temporal UAV-based multispectral vegetation indices and end-member abundance in rice. Field Crop Res. 2023;299:14.
58. Luo SJ, Jiang XQ, Jiao WH, Yang KL, Li YJ, Fang SH. Remotely sensed prediction of rice yield at different growth durations using UAV multispectral imagery. Agriculture-Basel. 2022;12:17.
59. Yuan WS, Meng Y, Li Y, Ji ZG, Kong QM, Gao R, et al. Research on rice leaf area index Estimation based on fusion of texture and spectral information. Comput Electron Agric. 2023;211:18.
60. Yang KL, Gong Y, Fang SH, Duan B, Yuan NG, Peng Y, et al. Combining spectral and texture features of UAV images for the remote Estimation of rice LAI throughout the entire growing season. Remote Sens. 2021;13:20.
61. Liu SB, Jin XL, Bai Y, Wu WB, Cui NB, Cheng MH, et al. UAV multispectral images for accurate Estimation of the maize LAI considering the effect of soil background. Int J Appl Earth Obs Geoinf. 2023;121:21.
62. Ganaie MA, Hu MH, Malik AK, Tanveer M, Suganthan PN. Ensemble deep learning: A review. Eng Appl Artif Intell. 2022;115:18.
63. Park W, Leibon G, Rockmore DN, Chirikjian GS. Accurate image rotation using Hermite expansions. IEEE Trans Image Process. 2009;18:1988–2003.
64. Yue JB, Yang GJ, Tian QJ, Feng HK, Xu KJ, Zhou CQ. Estimate of winter-wheat above-ground biomass based on UAV ultrahigh-ground-resolution image textures and vegetation indices. ISPRS-J Photogramm Remote Sens. 2019;150:226–44.
65. Luo SJ, Jiang XQ, He YB, Li JP, Jiao WH, Zhang SL, et al. Multi-dimensional variables and feature parameter selection for aboveground biomass Estimation of potato based on UAV multispectral imagery. Front. Plant Sci. 2022;13:13.
66. Yamaguchi T, Sasano K, Katsura K. Improving efficiency of ground-truth data collection for UAV-based rice growth Estimation models: investigating the effect of sampling size on model accuracy. Plant Prod Sci. 2024;27:1–13.

Publisher's note